

Aperture-Shared Millimeter-Wave/Sub-6 GHz Dual-Band Antenna Hybridizing Fabry–Pérot Cavity and Fresnel Zone Plate

Jianfeng Zhu^{ID}, Student Member, IEEE, Yang Yang^{ID}, Senior Member, IEEE,
Shaowei Liao^{ID}, Senior Member, IEEE, and Quan Xue^{ID}, Fellow, IEEE

Abstract—This article presents an aperture-shared dual-band large frequency-ratio high gain antenna for sub-6 GHz and millimeter-wave (mm-wave) bands applications. Initially, the partially reflective surface (PRS) of the Fabry–Pérot cavity (FPC) antenna operating at the sub-6 GHz band is realized by using single-layered periodic grid patches while the opaque region of the mm-wave bandwaveband Fresnel zone plate (FZP) lens antenna is implemented by using periodic double-screen dipoles. Then, the PRS and the FZP lens are hybridized together and upgraded into a kind of composite metasurface, which simultaneously functions as the PRS of the sub-6 GHz FPC antenna and the mm-wave bandwaveband FZP lens with little dual-band mutual interference. Thus, the FPC antenna and the FZP lens can share the same aperture with high aperture reuse efficiency. Because the principles are based on the FPC resonance and the collimating FZP lens, high gains are achieved at both bands without a feeding network. Meanwhile, a dual-band large frequency-ratio antenna is designed as the feed. A prototype working at 3 and 28 GHz bands is designed, fabricated, and measured to verify the idea.

Index Terms—Dual-band, Fabry–Pérot, Fresnel zone plate (FZP) lens, large frequency ratio, millimeter-wave (mm-wave), sub-6 GHz.

I. INTRODUCTION

THE wireless industry faces overwhelming transmission speed and capacity demands while the current exhausted microwave spectrum cannot meet this requirement [1]–[3].

Manuscript received December 17, 2020; revised April 18, 2021; accepted May 9, 2021. Date of publication July 26, 2021; date of current version December 16, 2021. This work was supported in part by the National Natural Science Foundation of China under Grant 61871189 and in part by the Natural Science Foundation of Guangdong Province under Grant 2019A1515011999. (*Corresponding author: Shaowei Liao*)

Jianfeng Zhu is with the Guangdong Provincial Key Laboratory of Millimeter-Wave and Terahertz, School of Electronic and Information Engineering, South China University of Technology, Guangzhou 510641, China, also with the Pazhou Laboratory, Guangzhou 510330, China, and also with the School of Electrical and Data Engineering, University of Technology Sydney, Ultimo, NSW 2007, Australia.

Yang Yang is with the School of Electrical and Data Engineering, University of Technology Sydney, Ultimo, NSW 2007, Australia.

Shaowei Liao and Quan Xue are with the Guangdong Provincial Key Laboratory of Millimeter-Wave and Terahertz, School of Electronic and Information Engineering, South China University of Technology, Guangzhou 510641, China, and also with the Pazhou Laboratory, Guangzhou 510330, China (e-mail: liaoshaoWei@scut.edu.cn).

Color versions of one or more figures in this article are available at <https://doi.org/10.1109/TAP.2021.3098559>.

Digital Object Identifier 10.1109/TAP.2021.3098559

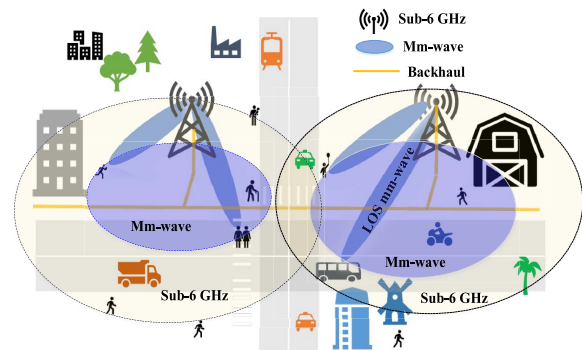


Fig. 1. Mm-wave/sub-6 GHz integrated 5G network.

Therefore, the millimeter-wave (mm-wave) spectrum has been exploited to tackle this issue. The general hurdles of this frequency range are the tremendous losses and the quasi-optical propagation path of communication link [4]–[6]. In fact, the mm-wave signal can only travel a few miles due to the severe propagation attenuation. Moreover, they are highly vulnerable to obstacles (cannot penetrate solid materials), making the mm-wave link highly intermittent. Hence, it is a real challenge to guarantee reliable communication since a mobile user will frequently experience blockage from vehicles, buildings, trees, and humans. To tackle this challenge, a reasonable and practical approach is to tightly integrate an mm-wave network with an existing sub-6 GHz network [7]–[10]. Contrary to the mm-wave signal, sub-6 GHz signals can propagate many miles and easily penetrate solid obstacles. Therefore, by adopting an mm-wave/sub-6 GHz integrated network, the lower frequency band can be used for providing a consistent and reliable user experience, while the higher frequency band can be used for large-volume data transmission with high speed, as illustrated in Fig. 1.

From the antenna technique point of view, separately placing two antennas respectively operating at sub-6 GHz and mm-wave is the easiest way but with low aperture reuse efficiency [11]–[14]. Instead, using an aperture-shared dual-band antenna that can simultaneously cover both mm-wave and sub-6 GHz is a better approach. Meanwhile, high gain is an indispensable feature of the antennas, not to mention the high path loss of the mm-wave band. Using an array formed by multiple antenna elements can achieve high gain,

albeit a rather bulky feeding network. An alternative approach to achieve high gain without a feeding network is using transmittarrays or lenses [15]–[27]. Apart from lenses, the Fabry–Pérot cavity (FPC) antenna also achieves high gain without a complicated feeding network. By employing a partially reflective surface (PRS) or nontransparent fully reflecting superstrate on top of a fully reflective surface with a low-directivity source, high directivity radiation can be achieved as long as the height of the cavity satisfies the resonant condition [28]–[35]. Although those approaches are efficient to achieve high gain, these antennas are limited in a single-band operation. How to employ these approaches to realize an aperture-shared high gain dual-band antenna that can simultaneously cover mm-wave and sub-6 GHz is still challenging. Recently, shared aperture dual-band antenna designs for sub-6 GHz and mm-wave applications have been proposed in [36] and [37], where the substrate-integrated-waveguide (SIW) slot antennas operating at the mm-wave band also functions as the radiator at sub-6 GHz with high aperture reuse efficiency. Nevertheless, the disadvantages are the relatively complicated feeding network for the mm-wave band and the low gain of the patch antenna for the sub-6 GHz band. To the best of our knowledge, large frequency-ratio antennas that achieve high gain at both sub-6 GHz and mm-wave bands simultaneously with high aperture reuse efficiency are rarely reported according to the open literature.

This article proposes a dual-band large frequency-ratio high gain antenna with high aperture reuse efficiency for the sub-6 GHz and mm-wave applications by hybridizing the FPC antenna and the Fresnel zone plate (FZP) lens together. The frequencies are adopted centering at 3 GHz for the sub-6 GHz band and 28 GHz for the mm-wave band for demonstration. Initially, the PRS of the FPC antenna is realized by using single-layered periodic grid patches, which can provide sufficient reflection to form the FPC resonance. While the opaque region of the FZP lens at the 28 GHz band is implemented using periodic double-screen dipoles, which can reflect electromagnetic (EM) wave at mm-wave band efficiently. Then, the PRS of the FPC antenna and the FZP lens are hybridized together and upgraded into a kind of composite metasurface, which simultaneously functions as the PRS of the FPC antenna at the 3 GHz band and the FZP lens at the 28 GHz band without mutual interference. A dual-band large frequency-ratio patch radiator is designed as the source feed. The antenna can achieve a high gain of 15.0 and 20.4 dBi for the sub-6 GHz and the mm-wave bands respectively with high aperture reuse efficiency.

II. ANTENNA CONFIGURATION AND PRINCIPLE

The basic antenna configuration and working principle are shown in Fig. 2(a). The antenna consists of two substrates stacked in order. A kind of composite metasurface is printed in the top substrate (substrate 1), which simultaneously functions as the PRS of the FPC antenna at the sub-6 GHz band and the FZP lens at the mm-waveband, as shown in Fig. 2(b). A dual-band large frequency-ratio patch antenna is designed as the source feed in the bottom substrate (substrate 2), as shown

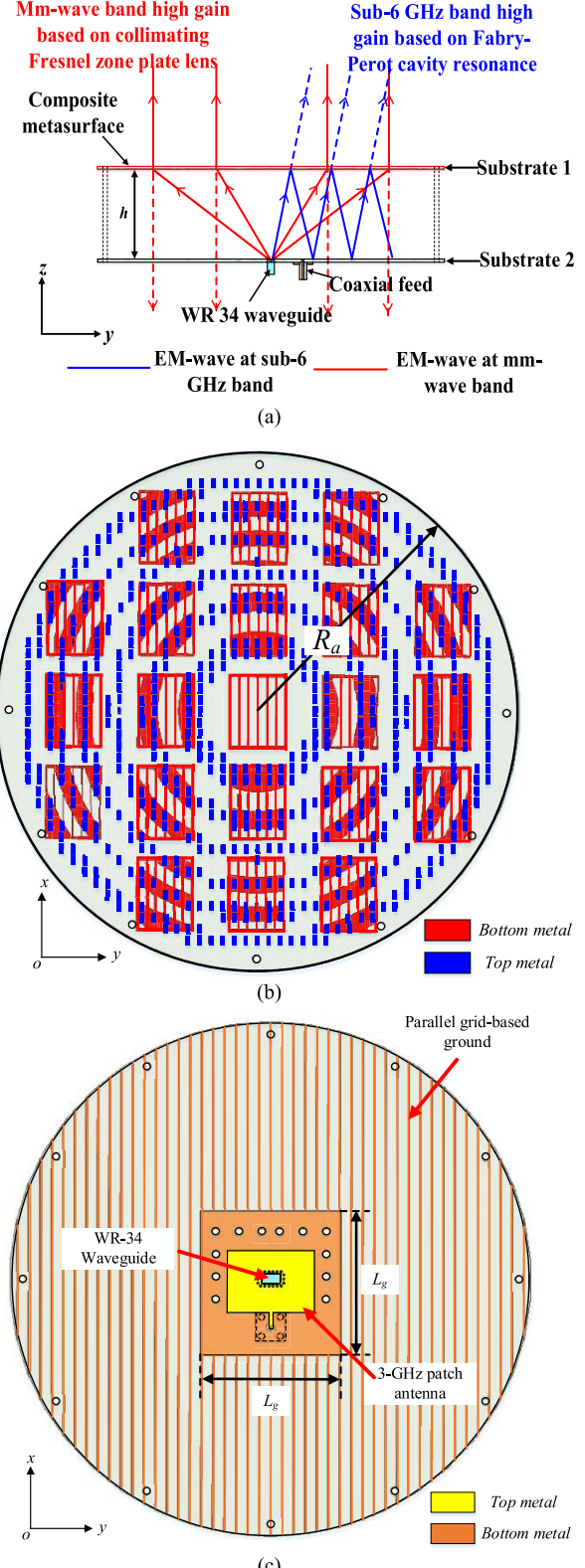


Fig. 2. Concept and configuration of the proposed dual-band large-frequency ratio high gain antenna. (a) Working principle (side view). (b) Top view of substrate 1 (composite metasurface). (c) Top view of substrate 2 (waveguide-integrated patch antenna mounted on parallel grid-based ground). ($h = 53$ mm, $R_a = 113$ mm, and $L_g = 63$ mm).

in Fig. 2(c). At the sub-6 GHz band, the EM wave radiated from the source feed is reflected multiple times inside the FPC, which interferes constructively in the broadside direction,

leading to a high gain. Meanwhile, at the mm-wave band, the EM wave from the source feed is collimated by the FZP lens with high directivity. In this way, the FPC antenna operating at the sub-6 GHz band and the FZP lens operating at the mm-waveband share the same aperture with high aperture reuse efficiency. More importantly, high gains are achieved at both bands without a feeding network. Considering that half of the energy reflected by the FZP lens reflects back and forth between the composite metasurface and the ground, resulting in a considerable gain variation at the mm-wave band, the ground of the FPC antenna is upgraded into a grid-based one. It allows EM wave at the mm-wave band to pass while reflects EM wave at the sub-6 GHz. The frequencies are adopted centering at 3 GHz for the sub-6 GHz band and 28 GHz for the mm-waveband, respectively. Note that the design frequencies are only chosen for demonstration, which can be potentially adjusted to other frequencies with different frequency ratios.

III. SUB-6 GHZ /MM-WAVE COMPOSITE METASURFACE DESIGN

To realize the FPC and FZP hybridized aperture-shared high gain antenna, the most important part is the composite metasurface on the top, which should simultaneously function as the PRS of the sub-6 GHz FPC antenna and the mm-wave band FZP lens. Thus, the PRS of the FPC antenna and the FZP lens are considered independently. Then, two structures are placed together, and further upgraded to reduce the mutual interference between them, forming the proposed composite metasurface, as shown in Fig. 2(b).

A. PRS of the FPC Antenna Operating at the 3 GHz Band

The PRS of the FPC antenna is considered first, which is implemented initially by arranging single-layer periodic patches on the surface of the Rogers 4003 substrate with a thickness of 1.524 mm, as depicted in Fig. 3(a). The corresponding geometric parameters are given in the caption of Fig. 3. Because of the half-wavelength resonance, the patch will reflect the x -polarized EM wave whose dielectric wavelength is twice the length of the patch. Adjacent to the half-wavelength resonant frequency, the reflection magnitude will gradually decrease and can be used as the PRS of the FPC antenna. The reflection magnitude and phase of the single-layer periodic patches are obtained in ANSYS HFSS using periodic boundary conditions (PBCs), as shown in Fig. 3(b). The half-wavelength resonance is located at 5 GHz with a reflection magnitude near 1. Then, at 3 GHz, the reflection magnitude is decreased to around 0.85, which is suitable to be used as the PRS of the FPC antenna. Generally, the directivity (D) of the FPC antenna and the reflection magnitude ($|\Gamma|$) of the PRS layer can be expressed as [38], [39]

$$D = 10 \log \frac{1 + |\Gamma|}{1 - |\Gamma|}. \quad (1)$$

Thus, the higher the reflection of the PRS, the higher the gain of the FPC antenna can achieve, but with a narrower

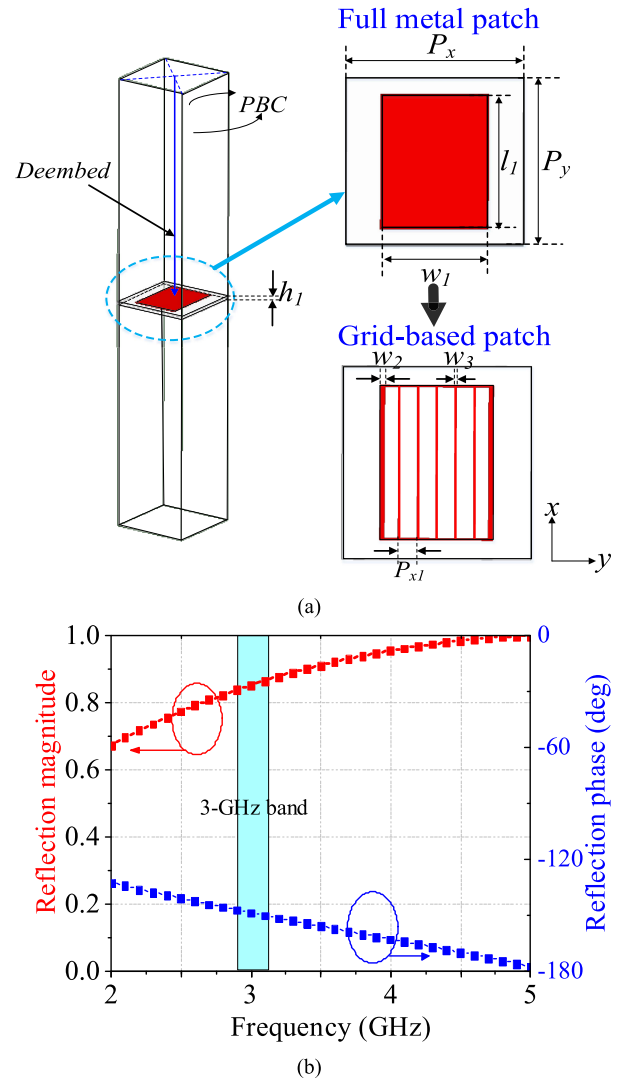


Fig. 3. (a) Configuration of the periodic patch and the grid-based patch forming PRS. (b) Reflection magnitude and phase of the periodic patch. ($h_1 = 1.524$ mm, $l_1 = 32$ mm, $w_1 = 24$ mm, $w_2 = 0.4$ mm, $w_3 = 0.2$ mm, $P_x = 40$ mm, $P_y = 40$ mm, and $P_{x1} = 4$ mm).

bandwidth. In the proposed design, the reflection magnitude of 0.85 is adopted merely for demonstration purposes since it can provide sufficient reflection to form the FPC resonance and maintain an acceptable bandwidth. Other reflection magnitudes can be also used based on the specific gain and bandwidth requirements.

Because the periodic patch operating at 3 GHz shares the same aperture with the FZP lens, it will block the 28 GHz band EM wave to pass, and thus destroying the collimating performance of the FZP lens. To avoid this, the full metal-based patch is upgraded into a kind of grid patch, as illustrated in Fig. 2(a). The advantage of using the parallel grid patch is that it can allow the EM wave at 28 GHz to pass. Meanwhile, the reflection performance remains the same as that of the full metal one at 3 GHz. The transmission performance of the parallel grid, whose simulation model is shown in Fig. 4, is investigated. As given in Fig. 5(a), the parallel grid prohibits the x -polarized 3 GHz EM wave while allowing the

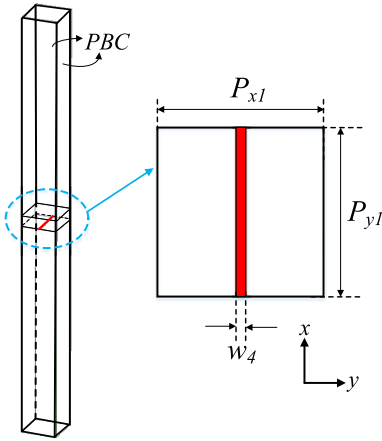


Fig. 4. Configuration of the proposed parallel grid unit forming grid-based patch. ($w_4 = 0.2$ mm, $P_{x1} = 4$ mm, and $P_{y1} = 4$ mm).

x -polarized 28 GHz band EM wave to pass. This is because the function of the parallel grids is determined by the period. If its period is long compared with the wavelength, the parallel grid functions as a diffraction grating and allows both x - and y -polarized wave to pass. However, when the parallel-grid spacing is much smaller than the wavelength, the parallel grid functions as a polarizer reflecting incident waves with polarization parallel to the parallel grid and transmits the EM wave of the orthogonal polarization [40]. Thus, the parallel grid can reflect the EM wave at the 3 GHz band along the x -direction and show little impact on the EM wave at 28 GHz passing through it. The transmission magnitude and phase of the 28 GHz band EM wave passing the Rogers 4003 substrate with and without the parallel grid are also given in Fig. 5. The transmission magnitude difference is less than 0.05 and the phase difference is around only 15° at the 28 GHz band. Thus, the parallel grid can be regarded as transparent to the EM wave at 28 GHz, i.e., its appearance has little impact on the 28 GHz EM wave passing through it. Then, the reflection performance comparisons of the full metal patch and the grid patch at the 3 GHz band are given in Fig. 6. The reflection magnitude and phase are nearly the same. This is understood that because the reflection is based on the half-wavelength resonance, the reflection property will not change much as long as the length of the patch (l_1) is fixed. Therefore, the performance of the FPC antenna operating at 3 GHz will maintain almost the same after using the proposed grid patch as the PRS.

As shown in Fig. 6, the reflection phase of the grid patch-based PRS is around -150° , which is important for determining the thickness of the FPC antenna. The thickness of the FPC antenna (h) should satisfy the Fabry–Pérot resonant condition, given by [28]

$$\frac{-4\pi h}{\lambda_0} + \varphi_{PRS} + \varphi_{Ground} = 2n\pi \quad (2)$$

where φ_{PRS} and φ_{Ground} are the reflection phases of the PRS and ground, respectively, λ_0 is the free space wavelength at the center frequency, and n is an integer. The initial value of h is 55.3 mm calculated based on (2). Then, h is further optimized

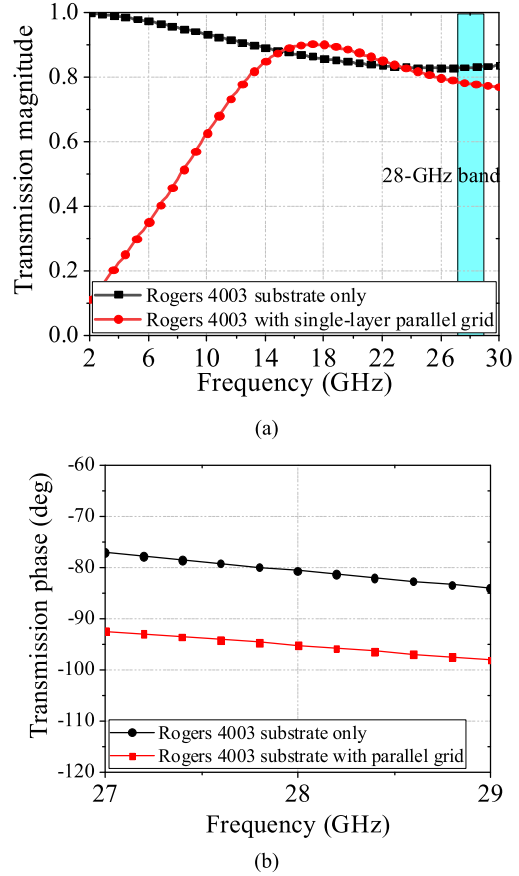


Fig. 5. Transmission performance comparison between the substrate with and without parallel grid. (a) Transmission magnitude. (b) Transmission phase.

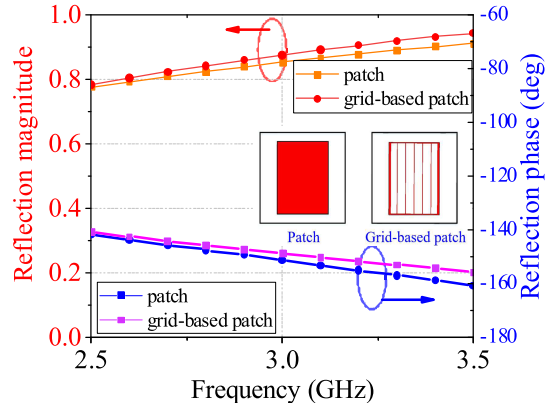


Fig. 6. Reflection magnitude and phase comparison between the periodic patch and periodic grid patch at 3 GHz band.

after the composite metasurface is incorporated. The reflection coefficients and realized gains at the 3 GHz band with different values of h when the composite metasurface is used as the PRS is given in Fig. 7. An h value of 53 mm is finally adopted with the good reflection coefficient and gain performance.

B. FZP Lens Operating at the 28 GHz Band

Now that the thickness of the antenna is determined, the FZP lens operating at the 28 GHz band can be designed.

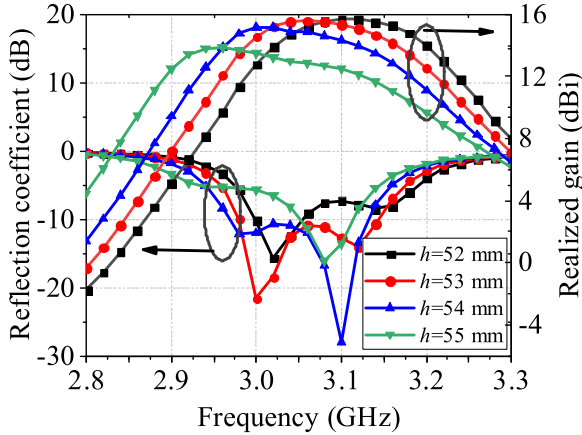


Fig. 7. Reflection coefficients and realized gains at 3 GHz band with different values of h when the composite metasurface is used as the PRS.

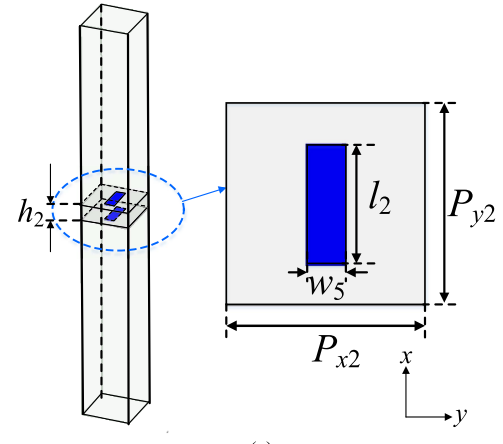
TABLE I
CALCULATED RADII OF THE FZP LENS

r_1	24.4mm	r_2	35.4mm	r_3	44.3mm
r_4	52.3mm	r_5	59.6mm	r_6	66.6mm
r_7	73.4mm	r_8	79.8mm	r_9	86.2mm
r_{10}	92.5mm	r_{11}	98.6mm	r_{12}	104.6mm

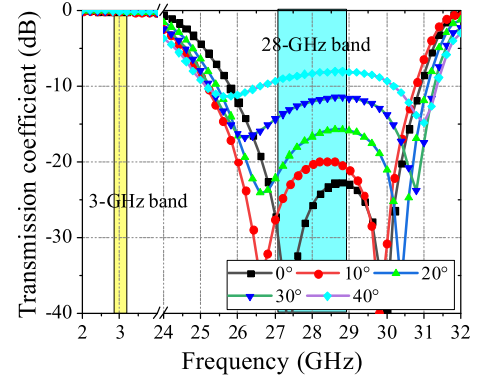
The radii (r_i) of each transparent and opaque zone can be determined by using [27]

$$r_i = \sqrt{i\lambda_0 F + \left(\frac{i\lambda_0}{2}\right)^2}, \quad i = 1, 2, \dots, N \quad (3)$$

where λ_0 is the design wavelength, and F is the focal length. The obtained radii of each zone of the FZP lens are given in Table I. Conventionally, the opaque annuli of the FZP lens are filled with full metal. Nevertheless, since the FZP also works as the PRS of the FPC antenna at the sub-6 GHz band in the proposed design, the opaque region of the FZP lens is filled with the periodic double-screen dipole. Unlike the full-metal structure, the periodic double-screen dipole can efficiently reflect the 28 GHz band EM wave while allowing the 3 GHz band EM wave to pass. The configuration of the double-screen dipole structure is given in Fig. 8(a). Because of the half-wavelength resonance, the double-screen dipole can reflect the x -polarized EM waves at the 28 GHz frequency band. Meanwhile, because its length is much smaller than the wavelength at 3 GHz, it is transparent to the 3 GHz EM wave, i.e., neither the transmission magnitude nor the transmission phase changes after the 3 GHz EM wave passing through the double-screen dipole. The transmission and reflection properties of the double-screen dipole are given in Fig. 8(b). It is seen that under the normal incident wave, the transmission coefficient is lower than -20 dB from 26.8 to more than 30 GHz, demonstrating that the double-screen dipole can efficiently reflect the EM wave. Meanwhile, at the 3 GHz band, the EM wave can transmit through the double-screen dipole structure freely. The reflection performance of the double-screen structure under different oblique incident angles is also given in Fig. 8(b). The transmission coefficient can maintain lower than -8 dB



(a)



(b)

Fig. 8. (a) Configuration of the double-screen dipole. ($h_2 = 1.524 \text{ mm}$, $l_2 = 3 \text{ mm}$, $w_5 = 1 \text{ mm}$, $P_{x2} = 5 \text{ mm}$, and $P_{y2} = 5 \text{ mm}$.) (b) Simulated transmission coefficient of the double-screen dipole under different incident angles.

when the incident angle reaches 40° , and the transmission coefficients at 3 GHz are nearly constant under different incident angles.

C. Hybrid Design

Since the 3 GHz band FPC antenna and the 28 GHz band FZP lens antenna share the same aperture, the PRS in Section III-A and FZP lens antenna in Section III-B are hybridized together, forming a kind of composite metasurface, as depicted in Fig. 9. After hybridization, there are four domains in the composite metasurface aperture, namely, Domain I: allows both 3 and 28 GHz band EM wave to pass (substrate only); Domain II: prohibits 28 GHz band EM wave and allows 3 GHz band EM wave to pass (substrate with the double-screen dipoles); Domain III: prohibits 3 GHz band EM wave and allows 28 GHz band EM wave to pass (substrate with single-layer parallel grids); and Domain IV: prohibits both 3 and 28 GHz band EM wave, presented by substrate with full metal. Thus, the composite metasurface is upgraded into the structure shown in Fig. 9(c). The achieved reflection coefficient and boresight realized gain comparisons at the 3GHz band by using the full metal patch, the grid patch,

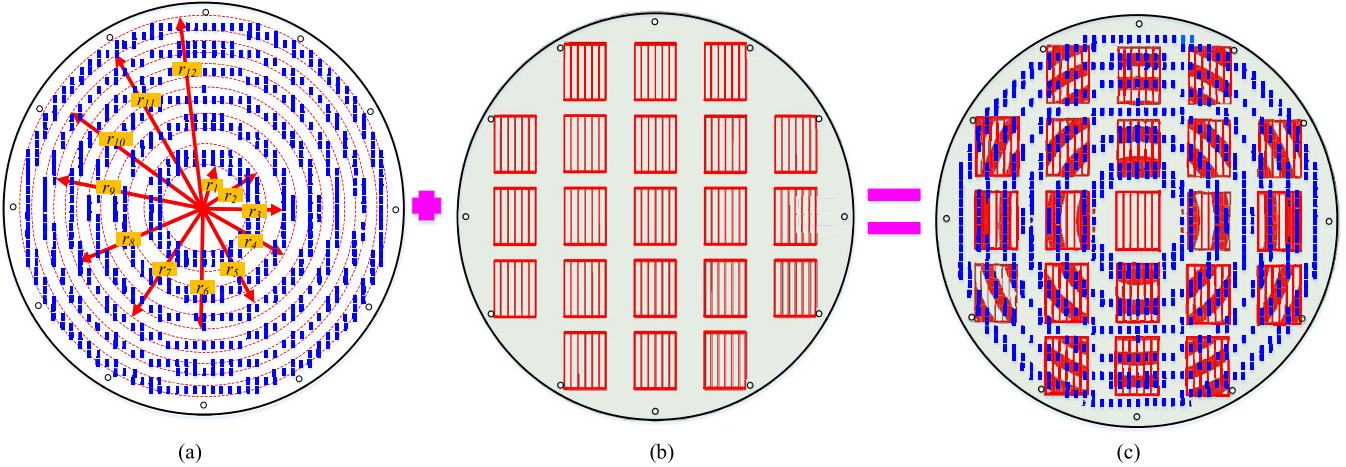


Fig. 9. (a) Double-screen dipole-based FZP lens. (b) Periodic grid patch-based PRS. (c) Double-screen dipole-based FZP lens and periodic grid patch-based PRS are hybridized together, forming the proposed composite metasurface.

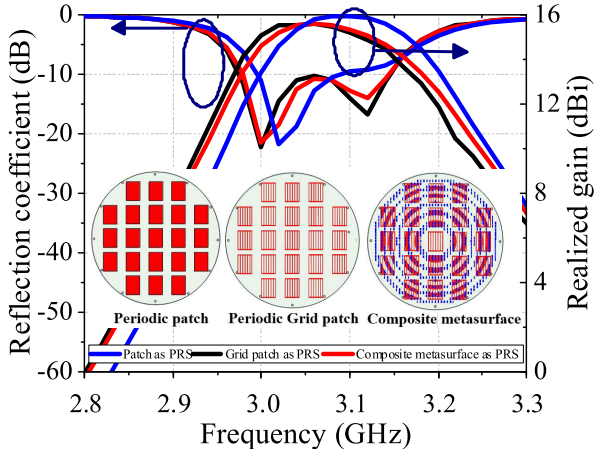


Fig. 10. Simulated boresight realized gain achieved using the periodic patch, the grid patch, and the composite metasurface as the PRS.

and the composite metasurface as the PRS are given in Fig. 10. The achieved boresight gains are nearly the same. The curve slightly shifts around 50 MHz to the lower band when the composite metasurface is used as the PRS. The achieved reflection coefficient and boresight gain comparisons at the 28 GHz band by using the double-screen dipole-based FZP lens [shown in Fig. 9(a)] and the composite metasurface-based FZP lens are given in Fig. 11. The achieved boresight realized gains are also nearly the same and the gain variation over the frequency band is less by using the proposed composite metasurface.

To better clarify the concept and the principles of the composite metasurface operating at the sub-6 GHz and mm-wave bands, the field distributions and comparisons in both bands are given respectively. First, the antenna's electric field distributions using the periodic patch, the grid patch, and the composite structure as the PRS at 3 GHz are given in Fig. 12. It is observed that the electrical field distributions of the three cases are nearly the same, demonstrating that the function of the proposed composite metasurface as the PRS is almost

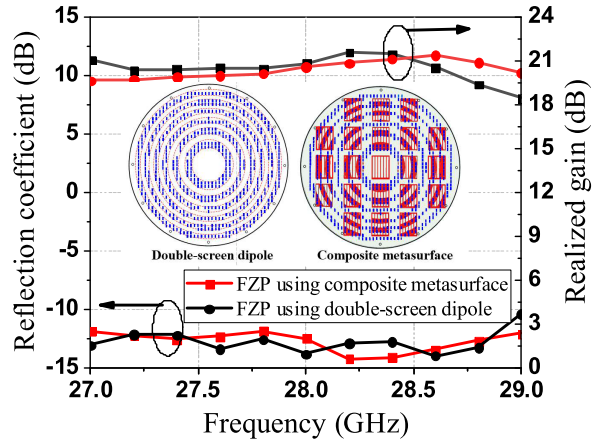


Fig. 11. Simulated boresight realized gain of the FZP lens using periodic double-screen dipole and using the composite metasurface.

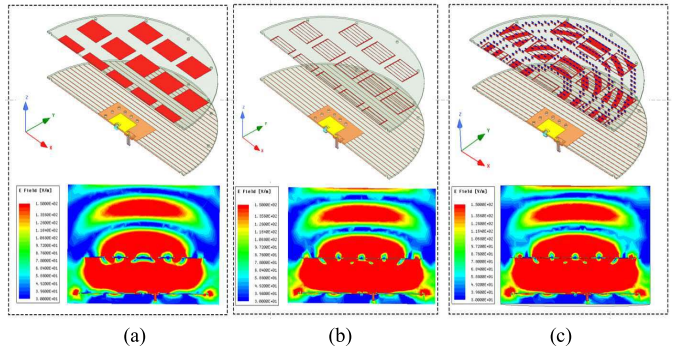


Fig. 12. Electric field distributions in xoz plane at 3 GHz. (a) Periodic patch as the PRS. (b) Grid patch as the PRS. (c) Composite metasurface as the PRS.

the same as that of the periodic patch. Second, the antenna's electric field distributions using the periodic dipole structure as the FZP and using the composite structure as the FZP at the mm-wave band are plotted in Fig. 13. Similar fields can be observed between the two cases. Together with the overall performance including radiation patterns and gain comparisons

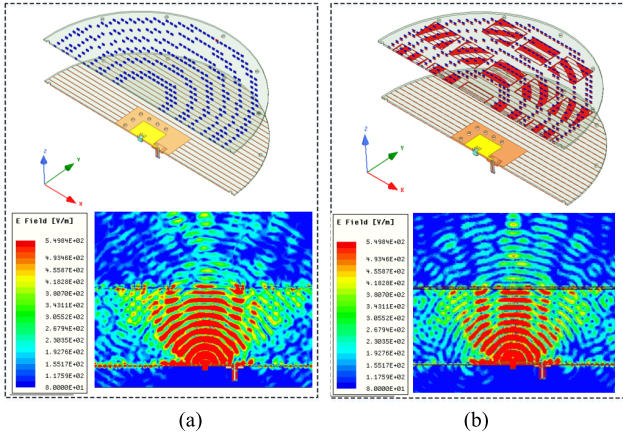


Fig. 13. Electric field distributions in xoz plane at 28 GHz. (a) Periodic double-screen dipole as the FZP. (b) Composite metasurface as the FZP.

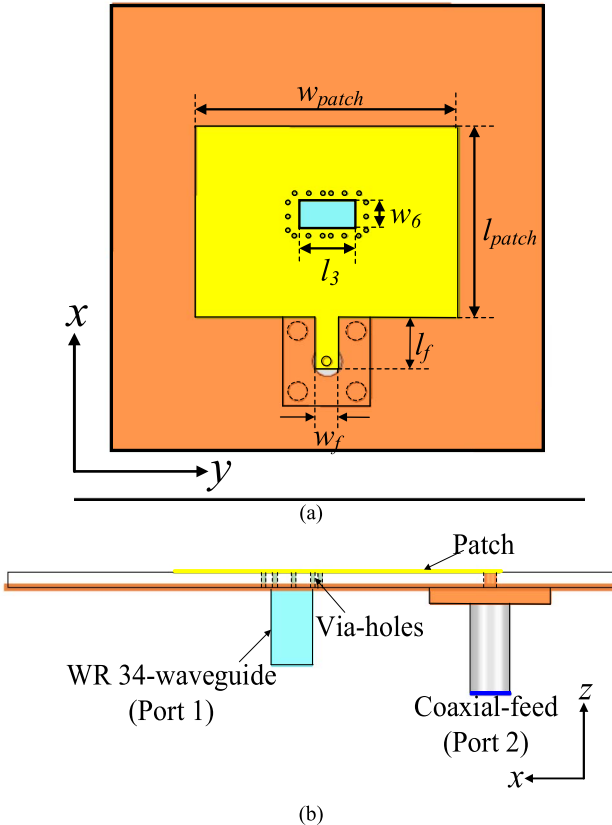


Fig. 14. Configuration of proposed waveguide-integrated patch radiator as primary feed. (a) Top view. (b) Side view. ($l_{patch} = 27.2$ mm, $w_{patch} = 37.2$ mm, $w_f = 3.2$ mm, $l_f = 6.88$ mm, $l_3 = 8$ mm, and $w_6 = 4$ mm).

in Figs. 10 and 11, the composite structure can function as the PRS of the FPC antenna at the 3 GHz band and the FZP antenna at the 28 GHz band.

IV. ANTENNA FEED AND GROUND DESIGN

A dual-band large frequency-ratio waveguide-integrated patch radiator is designed as the feed on Rogers 4003 substrate with a thickness of 1.524 mm, as shown in Fig. 14. The corresponding geometric parameters of the radiator are also given in the caption of Fig. 14. The traditional patch antenna

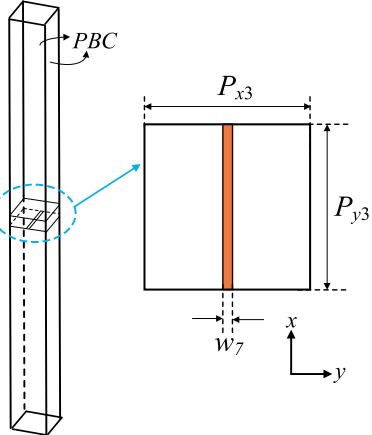


Fig. 15. Configuration of the proposed parallel grid to form the ground. ($w_7 = 0.4$ mm, $P_{x3} = 5$ mm, and $P_{y3} = 5$ mm).

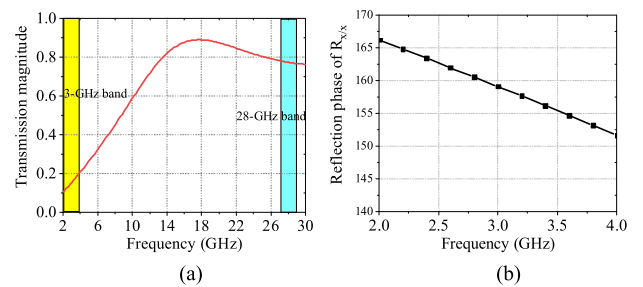


Fig. 16. (a) Transmission magnitude of the parallel grid. (b) Reflection phase of x -polarized incident wave at 3 GHz band.

is used as the 3 GHz band radiation. For the 28 GHz band radiation, slots are cut at the center of both the patch and the ground, and the slot on the ground is directly connected to a WR-34 waveguide, forming an open waveguide antenna. The slot is enclosed by metal vias to ensure the EM wave transmits through the substrate and radiated to the upper free space. Because half of the energy at the 28 GHz band is reflected back by the composite metasurface, the ground is implemented by using the parallel grid-based one, as shown in Fig. 2(c). The unit configuration of the grid is given in Fig. 15, and its transmission magnitude and reflection phase are given in Fig. 16. It is seen from Fig. 16 that the grids reflect the 3 GHz band EM wave with a reflection phase around 160° while the 28 GHz band EM wave can transmit through it. If a full metal ground is used, the reflected 28 GHz band EM wave will be reflected back and forth between the ground and composite metasurface, resulting in a large gain variation over the 28 GHz frequency band. As shown in Fig. 17, the gain variation is larger than 5 dB over the frequency from 27 to 29 GHz if the full metal ground is used. While the gain variation is less than 2 dB if the proposed parallel grid-based ground is used. The gain and reflection coefficient comparisons of the antenna at the sub-6 GHz band using the full-metal ground and using the parallel grid-based ground are also given in Fig. 18 for comparison. It is seen that the reflection coefficient of using the grid-based ground is better than the

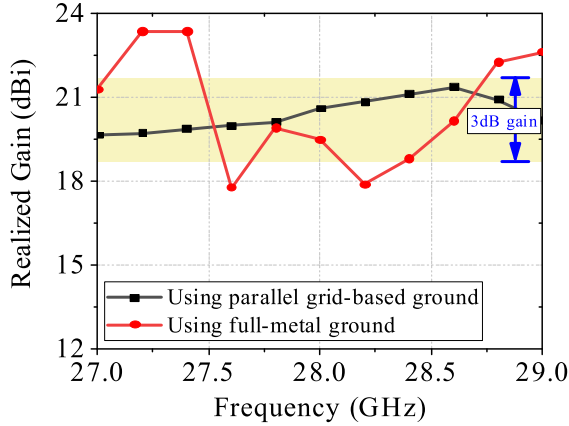


Fig. 17. Simulated boresight gain of the FZP lens with full metal ground and with parallel-grid based ground.

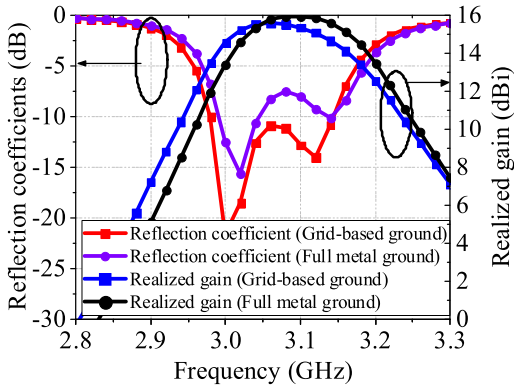


Fig. 18. Gain and reflection coefficient comparisons at 3 GHz band using the full-metal ground and using the parallel grid-based ground.

full-metal ground and the peak gain slightly shifts to the lower band by about 30 MHz.

V. ANTENNA MEASUREMENT AND DISCUSSION

The prototype of the antenna is fabricated, as shown in Fig. 19. The reflection coefficients of the antenna are given in Fig. 20. The -10 dB impedance bandwidth is from 2.97 to 3.13 GHz for the simulation and from 2.98 to 3.13 GHz for the measurement at the 3 GHz band. Because of the cut-off frequency of the waveguide, the isolation between the two ports is extremely high and is not shown in Fig. 20(a). For the mm-wave band, the simulated S_{11} of the antenna is below -12 dB and measured one below -10 dB. Some discrepancies mainly attribute to the fabrication tolerance and the connections between the vector network analyzer (VNA) cable and waveguide transition. Because the waveguide antenna and patch antenna share the same aperture, and two input ports are closely spaced, some mutual coupling is inevitable. Nevertheless, the mutual coupling is below -20 dB for simulation and below -17 dB for measurement. The radiation patterns at 3 and 3.05 GHz are given in Fig. 21(a) and (b), respectively. The radiation patterns agree well. The maximum gains are fixed at boresight with a symmetrical pattern. The sidelobes are lower than -15 dB and the cross-polarizations are better than

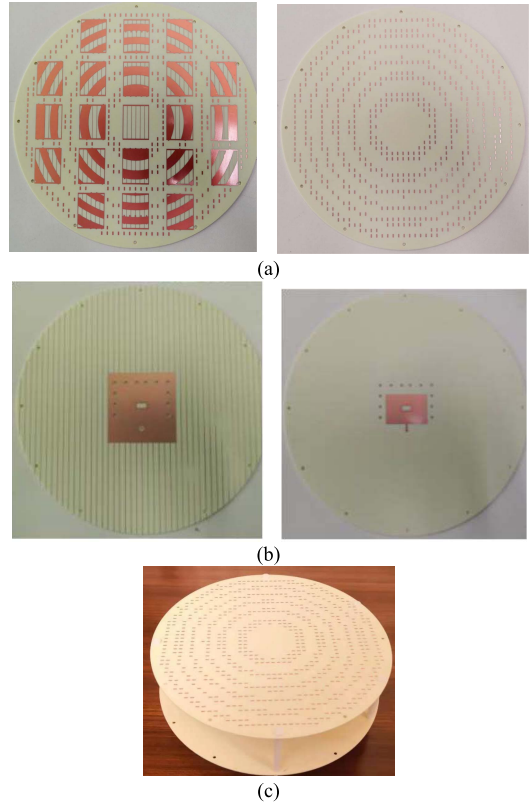


Fig. 19. Fabricated prototype. (a) Top view and bottom view of substrate 1. (b) Top view and bottom view of substrate 2. (c) Assembling view.

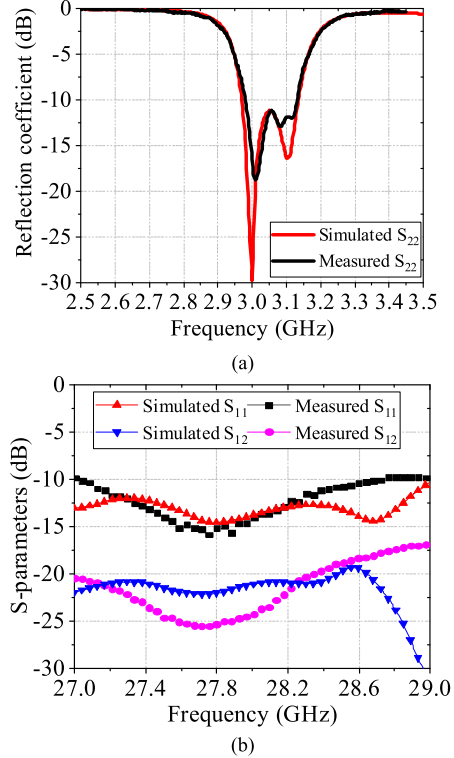


Fig. 20. S-parameters of the proposed antenna. (a) Simulated and measured S-parameters at 3 GHz band. (b) Simulated and measured S-parameters at 28 GHz band.

30 dB. The radiation patterns at 27, 28, and 29 GHz are given in Fig. 22(a), (b), and (c), respectively. The simulated and measured radiation patterns also agree well and the sidelobes

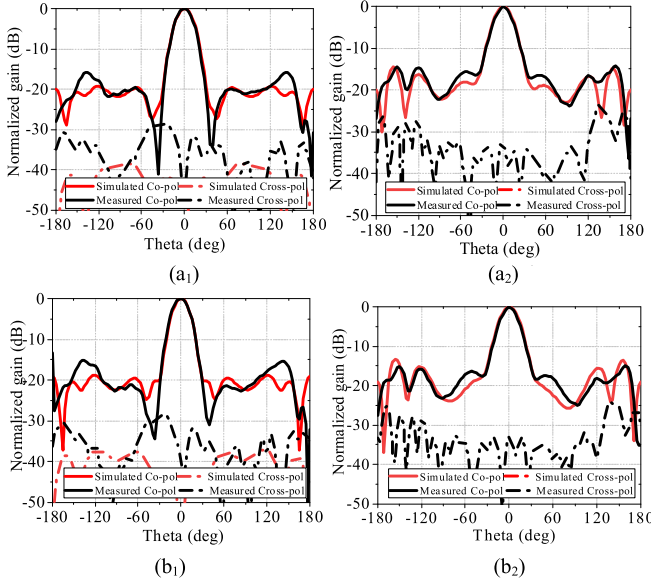


Fig. 21. Simulated and measured radiation patterns at (a) 3 and (b) 3.05 GHz. (a₁) xoz plane. (a₂) yoz plane. (b₁) xoz plane. (b₂) yoz plane.

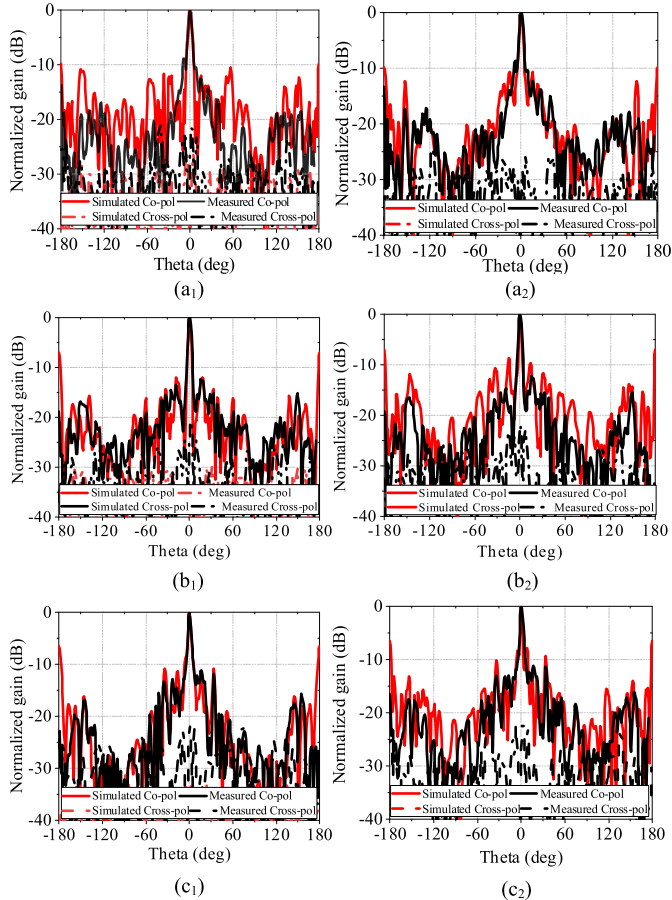


Fig. 22. Simulated and measured radiation patterns at (a) 27, (b) 28, and (c) 29 GHz. (a₁) xoz plane. (a₂) yoz plane. (b₁) xoz plane. (b₂) yoz plane. (c₁) xoz plane. (c₂) yoz plane.

of the patterns are low than -10 dB and the cross-polarizations are better than 20 dB. It is worth mentioning that the radiation at the mm-wave band has a high back lobe level because the FZP only allows the in-phase EM wave to pass and reflects

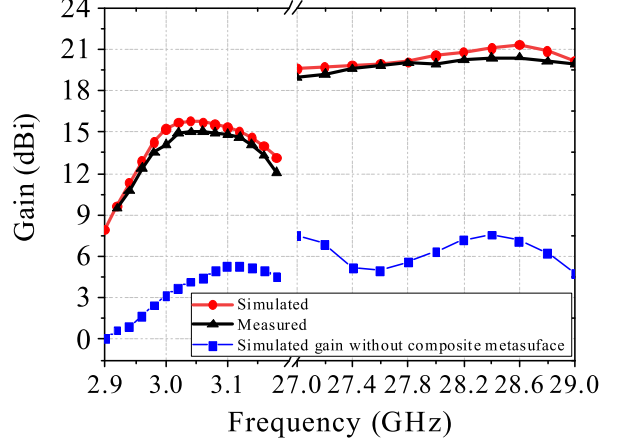


Fig. 23. Simulated and measured antenna gain.

the out-of-phase part, as depicted in Fig. 2(a). The simulated and measured gains are given in Fig. 23. The measured peak gain can achieve 15 and 20.4 dBi for the 3 and 28 GHz bands, respectively. Compared with the source feed, 10 and 14.5 dBi improvements are, respectively, observed for the 3 and 28 GHz bands after the composite metasurface is used.

Table II lists the comparison of the proposed design with the other dual-band/multi-band large frequency-ratio antennas operating at microwave and mm-wave bands. State-of-the-art works can be categorized into two kinds: one kind is using two separate antennas respectively operating at microwave band and mm-wave band [10]–[14]. These antennas feature the advantage of easy configuration and reduced design complexity, but with the disadvantage of low aperture efficiency. Using a shared aperture antenna operating at the sub-6 GHz and mm-wave simultaneously can improve the aperture reuse efficiency, enabling the system more compact. Recently, several interesting high aperture reuse efficiency antennas were proposed in [36] and [37] by using patch antenna for the sub-6 GHz radiation and simultaneously integrating SIW arrays into the patch antenna to achieve high gain radiation at the mm-wave band. Nevertheless, due to the restricted aperture size of the patch, the gain achieved at the sub-6 GHz band is low. Meanwhile, the design requires a relatively complicated feeding network to implement the array antenna at the mm-wave band. Other antenna configurations are also proposed for sub-6 GHz and mm-wave band applications without a feeding network [41]–[43], but these designs cannot achieve high gain at both bands because of the limited aperture size. In the proposed design, high gain is achieved at both the sub-6 GHz and mm-wave bands with an enlarged antenna aperture size. Because the high gain is achieved by exploiting the FPC resonance principle and the collimating FZP lens antenna for the sub-6 GHz and mm-wave bands, no feeding network is required. The design achieves high aperture reuse efficiency and is implemented by only stacking two PCB substrates in order, which maintains low fabrication and assembling cost. It is worth mentioning that the low aperture efficiency of mm-wave band results from the inherent drawback of the metallic FZP lens. To improve the aperture efficiency, the FZP

TABLE II
COMPARISON OF DIFFERENT KINDS OF DUAL-BAND/MULTIBAND ANTENNA FOR MICROWAVE AND MM-WAVE APPLICATIONS

Ref.	Freq (GHz)	Antenna type	Peak gain (dBi)	Array (Sub-6 GHz/mm-wave)	Reuse efficiency	Remarks
[11]	2.4/5.2/60	Monopole/grid array	1.9/3.4/16	No/Yes	0	Tri-band, compact size, high-gain at mm-wave band, feeding network required
[12]	4/60	Monopole/patch	4/7	No/No	0	Compact size, low gain, high isolation, no feeding network
[13]	5.8/30	Annular ring/SIW slot	4.5/9.37	No/No	0	Compact size, low gain, no feeding network
[36]	3.5/60	Patch antenna/SIW slot array antenna	7.3/24	No/Yes	High	High aperture reuse efficiency, small aperture size, high-gain at mm-wave band, feeding network required
[37]	2.4/60	Patch antenna/SIW slot array antenna	8.0/27.8	No/Yes	High	High aperture reuse efficiency, small aperture size, high-gain at mm-wave band, feeding network required
[41]	2.4/5.2/60	PIFA/SIW leaky wave antenna	3.97/4.07/1 2.29	No/Yes	High	High aperture reuse efficiency, small aperture size, high-gain at mm-wave band, beam steering
[42]	2.4/24	Dielectric resonator antenna/Fabry-Perot cavity antenna	6.8/18.2	No/No	High	High aperture reuse efficiency, small aperture size, high-gain at mm-wave band, no feeding network required
[43]	2.4/24	Waveguide antenna/Fabry-Perot cavity antenna	7.3/11.5	No/No	High	High aperture reuse efficiency, small aperture size, no feeding network required
[44]	5.2/24	slot antenna /Dielectric resonator antenna	3.93/6.2	No/No	High	High aperture reuse efficiency, compact size, low gain, no feeding network required
[45]	3/30	Monopole/ taper slot antenna	2.92/13.09	No/No	Low	Compact size, low aperture reuse efficiency, end-fire radiation at mm-wave band, no feeding network
This work	3/28	FPC antenna and FZP lens antenna hybrid design	15.0/20.4	No/No	High	High aperture reuse efficiency, large aperture size, high gain at dual-bands, no feeding network

lens can be possibly replaced by a transmitarray with better phase correction. However, the layers used may be increased as well. For the FPC antenna operating at 3 GHz, some judiciously designed superstrate principles [31]–[33] can be potentially used to further improve the aperture efficiency. In this work, the main target is to propose a new strategy hybridizing the FPC antenna and FZP lens to realize an aperture-shared antenna simultaneously operating at the sub-6 GHz/mm-wave bands. Improving the aperture efficiency will be valuable future work to investigate.

VI. CONCLUSION

In summary, a large frequency-ratio, aperture-shared high gain antenna is proposed for sub-6 GHz and mm-wave applications. A kind of composite metasurface is proposed first, which simultaneously functions as the PRS of the FPC antenna at the sub-6 GHz and FZP at the mm-wave band without mutual interference. Then, a dual-band large frequency-ratio antenna is designed as the feed. High gain is achieved in both bands without a feeding network. The antenna can achieve a high gain of 15.0 and 20.4 dBi for the sub-6 GHz and mm-wave bands, respectively, with extremely high aperture reuse efficiency.

REFERENCES

- [1] X. Wang *et al.*, “Millimeter wave communication: A comprehensive survey,” *IEEE Commun. Surveys Tuts.*, vol. 20, no. 3, pp. 1616–1653, 3rd Quart., 2018.
- [2] S. A. Busari, K. M. S. Huq, S. Mumtaz, L. Dai, and J. Rodriguez, “Millimeter-wave massive MIMO communication for future wireless systems: A survey,” *IEEE Commun. Surveys Tuts.*, vol. 20, no. 2, pp. 836–869, 2nd Quart., 2017.
- [3] M. Agiwal, A. Roy, and N. Saxena, “Next generation 5G wireless networks: A comprehensive survey,” *IEEE Commun. Surveys Tuts.*, vol. 18, no. 3, pp. 1617–1655, 3rd Quart., 2016.
- [4] T. S. Rappaport *et al.*, “Millimeter wave mobile communications for 5G cellular: It will work!” *IEEE Access*, vol. 1, pp. 335–349, 2013.
- [5] I. F. Akyildiz, J. M. Jornet, and C. Han, “Terahertz band: Next frontier for wireless communications,” *Phys. Commun.*, vol. 12, pp. 16–32, Sep. 2014.
- [6] I. A. Hemadeh, K. Satyanarayana, M. El-Hajjar, and L. Hanzo, “Millimeter-wave communications: Physical channel models, design considerations, antenna constructions, and link-budget,” *IEEE Commun. Surveys Tuts.*, vol. 20, no. 2, pp. 870–913, 2nd Quart., 2018.
- [7] M. M. Kassem and M. K. Marina, “Future wireless spectrum below 6 GHz: A UK perspective,” in *Proc. IEEE DySPAN*, Sep. 2015, pp. 59–70.
- [8] H. Shokri-Ghadikolaei *et al.*, “Millimeter wave cellular networks: A MAC layer perspective,” *IEEE Trans. Commun.*, vol. 63, no. 10, pp. 3437–3458, Oct. 2015.
- [9] J. Deng, O. Tirkkonen, R. Freij-Hollanti, T. Chen, and N. Nikaein, “Resource allocation and interference management for opportunistic relaying in integrated mmWave/sub-6 GHz 5G networks,” *IEEE Commun. Mag.*, vol. 55, no. 6, pp. 94–101, Jun. 2017.

- [10] Y. Zhu, G. Zheng, L. Wang, K.-K. Wong, and L. Zhao, "Content placement in cache-enabled sub-6 GHz and millimeter-wave multi-antenna dense small cell networks," *IEEE Trans. Wireless Commun.*, vol. 17, no. 5, pp. 2843–2856, May 2018.
- [11] L. Zhang, K. Y. See, B. Zhang, and Y. P. Zhang, "Integration of dual-band monopole and microstrip grid array for single-chip tri-band application," *IEEE Trans. Antennas Propag.*, vol. 61, no. 1, pp. 439–443, Jan. 2013.
- [12] D. Wang and C. H. Chan, "Multiband antenna for WiFi and WiGig communications," *IEEE Antennas Wireless Propag. Lett.*, vol. 15, pp. 309–312, 2016.
- [13] B. J. Xiang, S. Y. Zheng, H. Wong, Y. M. Pan, K. X. Wang, and M. H. Xia, "A flexible dual-band antenna with large frequency ratio and different radiation properties over the two bands," *IEEE Trans. Antennas Propag.*, vol. 66, no. 2, pp. 657–667, Feb. 2018.
- [14] F. Xiao, X. Lin, and Y. Su, "Dual-band structure-shared antenna with large frequency ratio for 5G communication applications," *IEEE Antennas Wireless Propag. Lett.*, vol. 19, no. 12, pp. 2339–2343, Dec. 2020, doi: [10.1109/LAWP.2020.3032739](https://doi.org/10.1109/LAWP.2020.3032739).
- [15] S. Liu *et al.*, "Free-standing metasurfaces for high-efficiency transmarrays for controlling terahertz waves," *Adv. Opt. Mater.*, vol. 4, no. 3, pp. 384–390, Mar. 2016.
- [16] C. Jouanlanne *et al.*, "Wideband linearly polarized transmitarray antenna for 60 GHz backhauling," *IEEE Trans. Antennas Propag.*, vol. 65, no. 3, pp. 1440–1445, Mar. 2017.
- [17] S.-W. Qu, H. Yi, B. J. Chen, K. B. Ng, and C. H. Chan, "Terahertz reflecting and transmitting metasurfaces," *Proc. IEEE*, vol. 105, no. 6, pp. 1166–1184, Jun. 2017.
- [18] Z. H. Jiang, Y. Zhang, J. Xu, Y. Yu, and W. Hong, "Integrated broadband circularly polarized multibeam antennas using berry-phase transmitarrays for *ka*-band applications," *IEEE Trans. Antennas Propag.*, vol. 68, no. 2, pp. 859–872, Feb. 2020.
- [19] S. L. Liu, X. Q. Lin, Z. Q. Yang, Y. J. Chen, and J. W. Yu, "W-band low-profile transmitarray antenna using different types of FSS units," *IEEE Trans. Antennas Propag.*, vol. 66, no. 9, pp. 4613–4619, Sep. 2018.
- [20] M. Jiang, Z. N. Chen, Y. Zhang, W. Hong, and X. Xuan, "Metamaterial-based thin planar lens antenna for spatial beamforming and multi-beam massive MIMO," *IEEE Trans. Antennas Propag.*, vol. 65, no. 2, pp. 464–472, Feb. 2017.
- [21] J. Wang *et al.*, "Metantenna: When metasurface meets antenna again," *IEEE Trans. Antennas Propag.*, vol. 68, no. 3, pp. 1332–1347, Mar. 2020.
- [22] A. Aziz, F. Yang, S. Xu, and M. Li, "An efficient dual-band orthogonally polarized transmitarray design using three-dipole elements," *IEEE Antennas Wireless Propag. Lett.*, vol. 17, no. 2, pp. 319–322, Feb. 2018.
- [23] S. Karimkashi and A. A. Kishk, "Focusing properties of fresnel zone plate lens antennas in the near-field region," *IEEE Trans. Antennas Propag.*, vol. 59, no. 5, pp. 1481–1487, May 2011.
- [24] H. D. Hristov, L. P. Kamburov, J. R. Urumov, and R. Feick, "Focusing characteristics of curvilinear half-open fresnel zone plate lenses: Plane wave illumination," *IEEE Trans. Antennas Propag.*, vol. 53, no. 6, pp. 1912–1919, Jun. 2005.
- [25] H. D. Hristov, *Fresnel Zones in Wireless Links, Zone Plate Lenses, and Antennas*. Boston, MA, USA: Artech House, 2000.
- [26] Y. Fan, B.-L. Ooi, H. D. Hristov, and M.-S. Leong, "Compound diffractive lens consisting of fresnel zone plate and frequency selective screen," *IEEE Trans. Antennas Propag.*, vol. 58, no. 6, pp. 1842–1847, Jun. 2010.
- [27] H. Markovich, D. Filonov, I. Shishkin, and P. Ginzburg, "Bifocal Fresnel lens based on the polarization-sensitive metasurface," *IEEE Trans. Antennas Propag.*, vol. 66, no. 5, pp. 2650–2654, May 2018.
- [28] G. V. Trentini, "Partially reflecting sheet array," *IRE Trans. Antennas Propag.*, vol. AP-4, no. 4, pp. 666–671, Oct. 1956.
- [29] R. M. Hashmi and K. P. Esselle, "A class of extremely wideband resonant cavity antennas with large directivity-bandwidth products," *IEEE Trans. Antennas Propag.*, vol. 64, no. 2, pp. 830–835, Feb. 2016.
- [30] Y. Ge, K. P. Esselle, and T. S. Bird, "The use of simple thin partially reflective surfaces with positive reflection phase gradients to design wideband, low-profile EBG resonator antennas," *IEEE Trans. Antennas Propag.*, vol. 60, no. 2, pp. 743–750, Feb. 2012.
- [31] K. Dutta, D. Guha, C. Kumar, and Y. M. M. Antar, "New approach in designing resonance cavity high-gain antenna using nontransparent conducting sheet as the superstrate," *IEEE Trans. Antennas Propag.*, vol. 63, no. 6, pp. 2807–2813, Jun. 2015.
- [32] K. Dutta, D. Guha, and C. Kumar, "Theory of controlled aperture field for advanced superstrate design of a resonance cavity antenna with improved radiations properties," *IEEE Trans. Antennas Propag.*, vol. 65, no. 3, pp. 1399–1403, Mar. 2017.
- [33] K. Dutta, D. Guha, and C. Kumar, "Synthesizing aperture fields over the superstrate of resonance cavity antenna for modifying its radiation properties," *IEEE Antennas Wireless Propag. Lett.*, vol. 15, pp. 1677–1680, 2016.
- [34] K. Dutta, P. K. Mishra, S. Manna, A. Pal, and D. Guha, "Geometrical optics-based advanced design of an open cavity resonant antenna," *IEEE Antennas Wireless Propag. Lett.*, vol. 20, no. 3, pp. 322–326, Mar. 2021.
- [35] Q.-Y. Guo and H. Wong, "A millimeter-wave Fabry-Pérot cavity antenna using Fresnel zone plate integrated PRS," *IEEE Trans. Antennas Propag.*, vol. 68, no. 1, pp. 564–568, Jan. 2020, doi: [10.1109/TAP.2019.2937359](https://doi.org/10.1109/TAP.2019.2937359).
- [36] J. F. Zhang, Y. J. Cheng, Y. R. Ding, and C. X. Bai, "A dual-band shared-aperture antenna with large frequency ratio, high aperture reuse efficiency, and high channel isolation," *IEEE Trans. Antennas Propag.*, vol. 67, no. 2, pp. 853–860, Feb. 2019.
- [37] J. F. Zhang, Y. J. Cheng, and Y. R. Ding, "An S- and V-band dual-polarized antenna based on dual-degenerate-mode feeder for large frequency ratio shared-aperture wireless applications," *IEEE Trans. Antennas Propag.*, vol. 68, no. 12, pp. 8127–8132, Dec. 2020, doi: [10.1109/TAP.2020.2983769](https://doi.org/10.1109/TAP.2020.2983769).
- [38] R. Lian, Z. Tang, and Y. Yin, "Design of a broadband polarization-reconfigurable Fabry-Pérot resonator antenna," *IEEE Antennas Wireless Propag. Lett.*, vol. 17, no. 1, pp. 122–125, Jan. 2018.
- [39] P.-Y. Qin, L.-Y. Ji, S.-L. Chen, and Y. J. Guo, "Dual-polarized wideband Fabry-Pérot antenna with quad-layer partially reflective surface," *IEEE Antennas Wireless Propag. Lett.*, vol. 17, no. 4, pp. 551–554, Apr. 2018.
- [40] A. F. Kurtz, R. Sujatha, and M. I. Xiang-Dong, "Wire grid polarizer," U.S. Patent 6665119, Dec. 16, 2003.
- [41] Y. R. Ding and Y. J. Cheng, "A tri-band shared-aperture antenna for (2.4, 5.2) GHz Wi-Fi application with MIMO function and 60 GHz Wi-Gig application with beam-scanning function," *IEEE Trans. Antennas Propag.*, vol. 68, no. 3, pp. 1973–1981, Mar. 2020, doi: [10.1109/TAP.2019.2948571](https://doi.org/10.1109/TAP.2019.2948571).
- [42] L. Y. Feng and K. W. Leung, "Dual-fed hollow dielectric antenna for dual-frequency operation with large frequency ratio," *IEEE Trans. Antennas Propag.*, vol. 65, no. 6, pp. 3308–3313, Jun. 2017.
- [43] L. Y. Feng and K. W. Leung, "Dual-frequency folded-parallel-plate antenna with large frequency ratio," *IEEE Trans. Antennas Propag.*, vol. 64, no. 1, pp. 340–345, Jan. 2016.
- [44] Y.-X. Sun and K. W. Leung, "Substrate-integrated two-port dual-frequency antenna," *IEEE Trans. Antennas Propag.*, vol. 64, no. 8, pp. 3692–3697, Aug. 2016.
- [45] J.-X. Chen, S.-H. Cao, and X.-F. Zhang, "SPPs-shared dual-band antenna with large frequency ratio," *IEEE Access*, vol. 8, pp. 29132–29139, 2020, doi: [10.1109/ACCESS.2020.2969274](https://doi.org/10.1109/ACCESS.2020.2969274).



Jianfeng Zhu (Student Member, IEEE) was born in Changsha, China. He received the B.Eng. degree in communication engineering from the Beijing University of Posts and Telecommunications (BUPT), Beijing, China. He is currently pursuing the joint Ph.D. degree with BUPT and University of Technology Sydney (UTS), Ultimo, NSW, Australia.

From 2015 to 2018, he was a Research Assistant with the State Key Laboratory of Millimeter Waves, Department of Electronic Engineering, City University of Hong Kong, Hong Kong. He was with the South China University of Technology (SCUT), Guangzhou, China, with the research of LTCC and antenna-in-package. He has authored or coauthored more than 40 journal articles and conference papers. His current research includes THz/sub-THz beam shaping and 3-D printing.



Yang Yang (Senior Member, IEEE) was born in Bayannur and grew up in Hohhot, Inner Mongolia, China. He received the M.Eng., M.Sc., and Ph.D. degrees from the Department of Electrical and Computer Systems Engineering (ECSE), Monash University Clayton Campus, Melbourne, VIC, Australia, in 2007, 2008, and 2013, respectively.

He has three years industry experience at Rain Bird Australia, Deer Park, VIC, Australia, as an Asia Pacific GSP Engineer, from 2012 to 2015. In 2015, he returned to academia and served as a Senior Research Associate with the Centre for Collaboration in Electromagnetic and Antenna Engineering, Macquarie University, Sydney, NSW, Australia. In 2016, he joined the State Key Laboratory of Terahertz and Millimeter Waves, City University of Hong Kong, Hong Kong, as a Research Fellow. Since 2016, he has been with the University of Technology Sydney, Ultimo, NSW, Australia, where he is currently a Senior Lecturer and the Team Leader of Millimeter-Wave Integrated Circuits and Antennas. He has over 150 international peer-reviewed publications in microwave and millimeter-wave (mm-wave) circuits and antennas. His research interests include mm-wave and sub-terahertz technologies in 5G and biomedical applications.

Dr. Yang received the Corporate 2014 Global GSP Success Award (one globally). He is the Winner of the CST University Publication Award 2018, by CST, Dassault Systèmes. He is currently an Associate Editor of the IEEE ACCESS and an Area Editor (Track Editor) of the *Microwave and Optical Technology Letters*. He is also a Committee Member of MTT-28 Biological Effects and Medical Applications.



Shaowei Liao (Senior Member, IEEE) received the Ph.D. degree in electromagnetic fields and microwave technology from the University of Electronic Science and Technology of China (UESTC), Chengdu, China, in 2010.

In 2011, he joined the School of Electronic Engineering, UESTC, as a Lecturer. From 2011 to 2012, he was a Senior Research Associate with the Department of Electronic Engineering, City University of Hong Kong, Hong Kong. From 2012 to 2013, he was a Research Scientist with Bell Laboratories Research, Shanghai Bell, Shanghai, China, and Alcatel-Lucent, Shanghai. From 2013 to 2017, he was an Engineer with the State Key Laboratory of Millimeter Waves, City University of Hong Kong. He is currently an Associate Professor with the School of Electronics and Information Engineering, South China University of Technology, Guangzhou, China. He has authored or coauthored more than 30 articles in IEEE journals. He is a co-inventor of five granted U.S. and European patents. His current research interests include various antennas, microwave components, and computational electromagnetics.

Dr. Liao is the Winner of the 2017 H. A. Wheeler Applications Prize Paper Award. He is a reviewer for the IEEE TRANSACTIONS ON ANTENNAS AND PROPAGATION, IEEE ANTENNAS AND WIRELESS PROPAGATION LETTERS, and the IEEE MICROWAVE AND WIRELESS COMPONENTS LETTERS.



Quan Xue (Fellow, IEEE) received the B.S., M.S., and Ph.D. degrees in electronic engineering from the University of Electronic Science and Technology of China (UESTC), Chengdu, China, in 1988, 1991, and 1993, respectively.

In 1993, he joined the UESTC, as a Lecturer, where he became a Professor in 1997. From 1997 to 1998, he was a Research Associate and then a Research Fellow with The Chinese University of Hong Kong, Hong Kong. In 1999, he joined the City University of Hong Kong, Hong Kong, as a Chair Professor of microwave engineering, where he also served as the Associate Vice President for the Innovation Advancement and China Office, from 2011 to 2015, he was the Director for the Information and Communication Technology Center, and the Deputy Director for the State Key Laboratory of Millimeter Waves. In 2017, he joined the South China University of Technology, Guangzhou, China, where he is currently a Professor and also serves as the Dean for the School of Electronic and Information Engineering. He has authored or coauthored over 300 internationally refereed journal articles and over 130 international conference papers. He is a co-inventor of the 13 five granted Chinese patents and 15 granted U.S. patents, in addition with 26 filed patents. His current research interests include microwave/millimeter-wave/THz passive components, active components, antenna, microwave monolithic integrated circuits, monolithic microwave integrated circuit (MMIC), and radio frequency integrated circuits.

Dr. Xue was an AdCom Member of MTT-S from 2011 to 2013. He served as an Associate Editor for the IEEE TRANSACTIONS ON MICROWAVE THEORY AND TECHNIQUES from 2010 to 2013, the Editor for the *International Journal of Antennas and Propagation* from 2010 to 2013, and an Associate Editor for the IEEE TRANSACTIONS ON INDUSTRIAL ELECTRONICS from 2010 to 2015. Since 2016, he has been an Associate Editor of the IEEE TRANSACTIONS ON ANTENNAS AND PROPAGATION.